

Article

Effects of Fe/Si Stoichiometry on Formation of Fe₃Si/FeSi-Al₂O₃ Composites by Aluminothermic Combustion Synthesis

Chun-Liang Yeh ^{*}, Kuan-Ting Chen and Tzong-Hann Shieh

Department of Aerospace and Systems Engineering, Feng Chia University, Taichung 40724, Taiwan; m0825565@fcu.edu.tw (K.-T.C.); thshieh@fcu.edu.tw (T.-H.S.)

* Correspondence: clyeh@fcu.edu.tw; Tel.: +886-4-2451-7250 (ext. 3963)

Abstract: Aluminothermic combustion synthesis was conducted with Fe₂O₃-Al-Fe-Si reaction systems under Fe/Si stoichiometry from Fe-20 to Fe-50 at. % Si to investigate the formation Fe₃Si/FeSi-Al₂O₃ composites. The solid-state combustion was sufficiently exothermic to sustain the overall reaction in the mode of self-propagating high-temperature synthesis (SHS). Dependence of iron silicide phases formed from SHS on Fe/Si stoichiometry was examined. Experimental evidence indicated that combustion exothermicity and flame-front velocity were affected by the Si percentage. According to the X-ray diffraction (XRD) analysis, Fe₃Si-Al₂O₃ composites were synthesized from the reaction systems with Fe-20 and Fe-25 at.% Si. The increase of Si content led to the formation of both Fe₃Si and FeSi in the final products of Fe-33.3 and Fe-40 at.% Si reaction systems, and the content of FeSi increased with Si percentage. Further increase of Si to Fe-50 at.% Si produced the FeSi-Al₂O₃ composite. Scanning electron microscopy (SEM) images revealed that the fracture surface morphology of the products featured micron-sized and nearly spherical Fe₃Si and FeSi particles distributing over the dense and connecting substrate formed by Al₂O₃.



Citation: Yeh, C.-L.; Chen, K.-T.; Shieh, T.-H. Effects of Fe/Si Stoichiometry on Formation of Fe₃Si/FeSi-Al₂O₃ Composites by Aluminothermic Combustion Synthesis. *Metals* **2021**, *11*, 1709. <https://doi.org/10.3390/met11111709>

Academic Editor: Dmitrii E. Andreev

Received: 22 September 2021
Accepted: 23 October 2021
Published: 26 October 2021

Publisher's Note: MDPI stays neutral with regard to jurisdictional claims in published maps and institutional affiliations.



Copyright: © 2021 by the authors. Licensee MDPI, Basel, Switzerland. This article is an open access article distributed under the terms and conditions of the Creative Commons Attribution (CC BY) license (<https://creativecommons.org/licenses/by/4.0/>).

Keywords: iron silicides; composites; self-propagating high-temperature synthesis (SHS); aluminothermic reduction; combustion kinetics

1. Introduction

Transition metal silicides have been promising for a wide range of applications including microelectronic transistors, high-temperature structural components, thin film coatings, thermoelectrics, spintronic devices, and catalysts [1–6]. Of many transition metal silicides, iron silicides exhibit magnetic, semiconducting, metallic, and insulating characteristics, depending on different crystalline structures [7,8]. According to the Fe-Si phase diagram, Fe₃Si, FeSi, and β-FeSi₂ are stable at room temperature, whereas Fe₂Si, Fe₅Si₃, and α-FeSi₂ are metastable [9]. Moreover, Fe₃Si exists within a wide range of stoichiometry from 10 to 25 at.% Si, FeSi is stoichiometric in a very narrow composition range and both phases are coexistent in the range between 25 and 50 at.% Si [9,10].

Among various fabrication routes to prepare iron silicides in monolithic and composite forms, the reaction synthesis methods associated with mechanical alloying and combustion process have been of great interest. For example, FeSi and β-FeSi₂ were produced by mechanically-activated combustion reaction of the Fe + 2Si powder mixture pretreated by shock-assisted ball milling for a long period of time [11,12]. In addition to mechanical activation, Gras et al. [13] adopted KNO₃ of 20 wt.% to chemically promote self-sustaining combustion reaction of the Fe + 2Si mixture for the formation of FeSi and α-FeSi₂ composites. Zakeri et al. [14] conducted mechanical alloying of SiO₂ and Al powders with stainless steel balls for 45 h to fabricate FeSi-Al₂O₃ nanocomposite powders from induced reactions. According to Guan et al. [15], Fe₃Si-Al₂O₃ nanocomposites were produced from Fe₃O₄, Al, and Si reactant powders through 4-h mechanical alloying followed by an annealing process at 900 °C for 1 h. Besides, Li et al. [16] produced iron silicide nanoparticles of various phases by thermal annealing of Fe-FeSi₂ samples with a core-shell structure and identified

the phase transformation from Fe–FeSi₂ to FeSi and Fe₃Si under an annealing time of 2 h and temperatures of 600 and 700 °C. Recently, an in situ fabrication approach combining the chemical interaction between Fe and Si with aluminothermic reduction of Fe₂O₃ and SiO₂ has been attempted to produce FeSi–Al₂O₃ and α-FeSi₂–Al₂O₃ composites in the mode of self-propagating high-temperature synthesis (SHS) [17,18]. With the advantages of energy efficiency, rapid reaction, simplicity, and high-purity products [19], the SHS scheme has been recognized as one of the most effective methods for preparing transition metal silicides in monolithic and composite forms [20–23].

As an extension of the previous studies [17,18], this work aims to investigate the production of Fe₃Si/FeSi–Al₂O₃ composites by aluminothermite-based combustion synthesis in the SHS mode, with an emphasis on exploring the effect of Fe/Si stoichiometry on the formation of Fe₃Si and FeSi. So far, no studies have been reported in the literature on combustion synthesis of Fe₃Si which exists in a wide stoichiometric range from 10 to 25 at.% Si. In this work, the reactant mixtures with different Fe/Si stoichiometries were prepared for combustion experiments, reaction exothermicity and combustion wave kinetics of the SHS process were studied, and compositional and microstructural analyses of the final products were performed.

2. Materials and Methods

The starting materials used by this study included Fe₂O₃ (Alfa Aesar Co., Ward Hill, MA, USA, <45 μm, 99.5%), Al (Showa Chemical, Tokyo, Japan, <45 μm, 99.9%), Fe (Alfa Aesar Co., <45 μm, 99.5%), and Si (Strem Chemicals, Newburyport, MA, USA, <45 μm, 99.5%). The stoichiometric composition of the reactants and products is expressed as Reaction (1) with three variables x , m , and n .



The stoichiometric coefficient x was varied between 0.75 and 3.0 to examine the influence of Fe/Si stoichiometry on the formation of silicide phases. Specifically, Reaction (1) was carried out with $x = 0.75, 1.0, 1.5, 2.0,$ and 3.0 , i.e., the test specimens with Fe/Si stoichiometries of Fe-20, 25, 33.3, 40, and 50 at.% Si were formulated. According to the value of x , the coefficients m and n were calculated and summarized in Table 1.

Table 1. Stoichiometric coefficients (x , m , and n) of Reaction (1).

x	Stoichiometric Coefficients	
	m	n
0.75	1.5	0
1.0	1.5	0
1.5	1.125	1.125
2.0	0.75	2.25
3.0	0	4.5

Note that with respect to Fe₃Si, Reaction (1) with $x = 0.75$ represents an off-stoichiometric condition with a Si-lean mixture of Fe-20 at.% Si, under which the silicide phase to be produced is Fe₃Si owing to its wide formation stoichiometry. The Fe/Si proportions of Reaction (1) with $x = 1.0$ and 3.0 match the exact stoichiometries of Fe₃Si and FeSi, respectively; thus, they are expected to be the only silicide formed in the corresponding conditions. Based on the Fe-Si phase diagram, the products containing two silicide phases, Fe₃Si and FeSi, are considered for Reaction (1) with $x = 1.5$ and 2.0 in Table 1.

Calculation of the adiabatic combustion temperature (T_{ad}) was performed for Reaction (1) with $x = 1.0, 1.5, 2.0,$ and 3.0 by the following energy balance equation [17,18] and thermochemical data taken from [24,25].

$$\Delta H_r + \int_{298}^{T_{ad}} \sum n_j C_p(P_j) dT + \sum_{298-T_{ad}} n_j L(P_j) = 0 \quad (2)$$

where ΔH_r° is the reaction enthalpy at 298 K, n_j is the stoichiometric constant, C_p and L are the heat capacity and latent heat, and P_j refers to the product.

Reactant powders were well mixed and compressed into cylindrical samples with 7 mm in diameter, 10 mm in length, and a relative density of 55%. The relative density of the test specimen is related to its initial components. The theoretical density (ρ_{TD}) of the test specimen is calculated from the mass fraction (Y) and density (ρ) of each component through the following equation:

$$\frac{1}{\rho_{TD}} = \frac{Y_{Fe_2O_3}}{\rho_{Fe_2O_3}} + \frac{Y_{Al}}{\rho_{Al}} + \frac{Y_{Fe}}{\rho_{Fe}} + \frac{Y_{Si}}{\rho_{Si}} \quad (3)$$

The SHS experiment was conducted in a stainless steel combustion chamber equipped with two quartz viewing windows and filled with high-purity argon (99.99%, Hochun Gas Co., Taichung, Taiwan) at 0.25 MPa. Based upon the time sequence series of combustion images, the flame-front trajectory as a function of time was constructed. The time derivative of the trajectory was determined as the combustion wave velocity (V_f). To facilitate the accurate measurement of instantaneous locations of the combustion front, a beam splitter (Rolyn Optics Co., Covina, CA, USA), with a mirror characteristic of 75% transmission and 25% reflection, was used to optically superimpose a scale onto the image of the test sample. The flame-front propagation velocity was slightly higher in the early stage right after the ignition, and then the linearity of time derivative of the trajectory implied that propagation of the flame front can be treated as a constant-velocity event. The relatively high propagation velocity in the beginning was attributed to the thermal energy supplied by the igniter, and the constant velocity in the later stage represents self-sustained propagation of the flame front.

The combustion temperature was measured by a fine-wire thermocouple with a bead diameter of 125 μm . R-type thermocouples (Omega Engineering Inc., Norwalk, CT, USA) with an alloy combination of Pt/Pt-13%Rh were used. The thermocouple bead was firmly attached on the sample surface at a position ~ 5 mm below the ignition plane. At this location, self-sustaining combustion was well developed so that measurement of the combustion front temperature (T_c) was justified. Phase constituents of the end products were identified by an X-ray diffractometer (Bruker D2 Phaser, Billerica, MA, USA) with CuK_α radiation. Scanning electron microscopy (SEM, Hitachi, S3000H, Tokyo, Japan) examination and energy dispersive spectroscopy (EDS) analysis were performed to study the fracture surface microstructure and elemental composition of the final products. Details of the experimental methods were reported elsewhere [26].

3. Results and Discussion

3.1. Combustion Exothermicity and Combustion Wave Kinetics

Calculated ΔH_r° and T_{ad} of Reactions (1) with different values of x are presented in Figure 1. The calculation was based on the products with phase compositions specified by the values of m and n listed in Table 1. Results showed that the increase of x from 1.0 to 3.0 led to an increase of ΔH_r° from -881.9 to -1118.6 kJ for Reaction (1), but a decrease of T_{ad} from 3059 to 2872 K. The increase of ΔH_r° is caused by the fact that both the aluminothermic reduction of Fe_2O_3 and formation of iron silicides are heat-releasing reactions. Moreover, the number of moles of iron silicides (i.e., the sum of m and n) formed in the final product increases with increasing x value. Specifically, the reaction of $\text{Fe}_2\text{O}_3 + 2\text{Al} \rightarrow 2\text{Fe} + \text{Al}_2\text{O}_3$ is extremely exothermic with $\Delta H_r^\circ = -852.3$ kJ and the formation enthalpies of Fe_3Si and FeSi are -79.4 and -73.1 kJ/mol, respectively [24]. On the other hand, the decrease of T_{ad} was because the reaction exothermicity (i.e., $\Delta H_r^\circ/C_p$) of aluminothermic reduction of Fe_2O_3 is much higher than that of the formation of Fe_3Si and FeSi . Consequently, the combustion temperature of the overall reaction decreased as the molar fraction of iron silicides in the product increased.

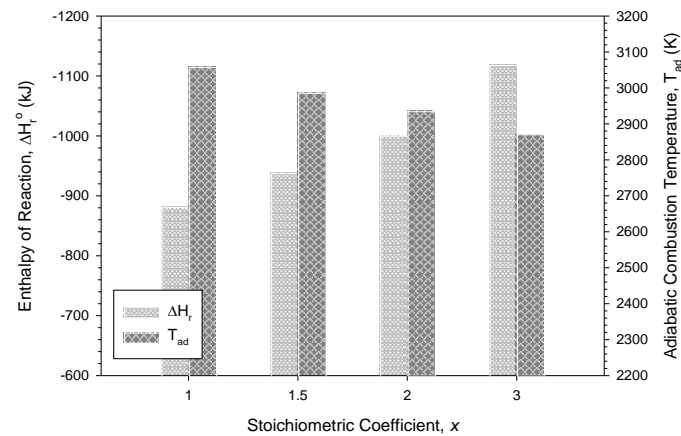


Figure 1. Enthalpy of reaction (ΔH_r°) and adiabatic combustion temperature (T_{ad}) of Reaction (1) with different stoichiometric coefficients, x .

As calculated adiabatic temperatures are higher than the criterion proposed by Merzhanov [19], combustion synthesis based on Reaction (1) is thermally satisfactory to be self-sustaining. Besides thermodynamic considerations, the SHS process must overcome the kinetic limitation of the reaction. Kinetic restraints are caused by inadequate reactivity owing to the presence of diffusion barriers. It is believed that the reduction of Fe_2O_3 by Al to produce Fe and Al_2O_3 acts as the initiation step, followed by the interaction between Fe and Si to generate FeSi and/or Fe_3Si [27].

Figure 2 illustrates a representative sequence of combustion images recorded from Reaction (1) with $x = 1.5$. It is evident that upon ignition a well-defined combustion front forms and propagates along the powder compact in a self-sustaining style. The progression of combustion wave arrived at a nearly constant rate after the ignition energy was faded out and the high exothermicity of combustion caused partial melting of the burned sample.

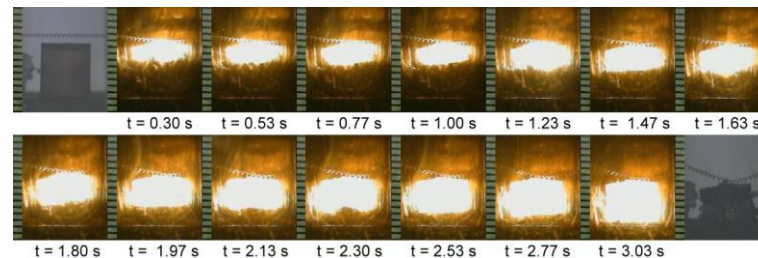


Figure 2. A time series of recorded images illustrating self-propagating combustion wave of Reaction (1) with $x = 1.5$ (unit of scale bar: 1 mm).

The measured combustion wave velocity reported in Figure 3a decreases from about 2.7 to 1.6 mm/s when the value of x increases from 0.75 to 3.0. The decline of combustion front speed was mainly ascribed to the dilution effect of Fe and Si additions and to the increase of iron silicides formed in the product. The combustion wave propagation rate is mostly governed by the layer-by-layer heat transfer from the reacting region to unburned zone and is likely affected by the combustion front temperature. Typical temperature profiles of Reaction (1) under different stoichiometries are depicted in Figure 3b. The temperature profile suggested that the sample experienced a steep thermal gradient and a rapid cooling rate, both of which are SHS characteristics. The peak value of the profile was defined as the combustion front temperature (T_c). As shown in Figure 3b, the value of T_c decreased from 1730 °C at $x = 0.75$ to 1506 °C at $x = 3.0$, confirming the dilution effect on combustion with Fe and Si additions. It is important to note that the dependence of combustion front temperature on Fe/Si stoichiometry was in a manner consistent with that of combustion wave velocity. The descending trend of T_c with x value is in agreement

with that of T_{ad} . However, because burning samples suffered considerable heat losses to surrounding argon by conduction and convection and to the inner wall of the chamber by radiation, the measured T_c was lower than the calculated T_{ad} .

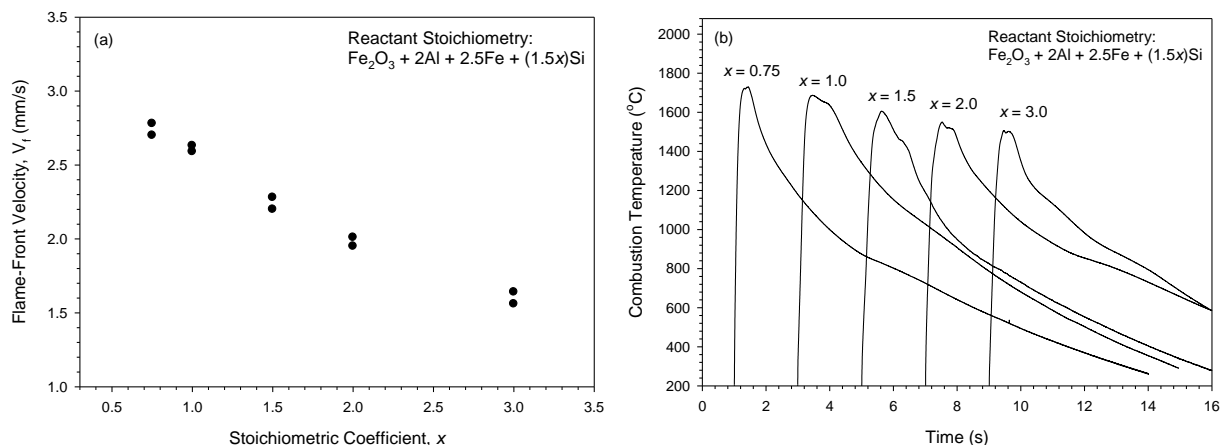


Figure 3. Effects of stoichiometric coefficient x on (a) flame-front propagation velocity and (b) combustion temperature.

3.2. Composition and Microstructure of Synthesized Products

Figure 4a,b plots XRD patterns of two products respectively produced from Reaction (1) with $x = 0.75$ and 1.0. As indicated in Figure 4a, the formation of Fe_3Si and Al_2O_3 with almost no other phases was obtained from an off-stoichiometric and Si-lean sample of Fe-20 at.% Si (i.e., $x = 0.75$). For Reaction (1) with Fe/Si stoichiometry of Fe-25 at.% Si (i.e., $x = 1.0$), Figure 4b reveals that in addition to two target compounds, Fe_3Si and Al_2O_3 , a minor compound, aluminum silicate or mullite, was found. Mullite is a stable solid solution in the Al_2O_3 - SiO_2 system and refers to $Al_{4+2z}Si_{2-2z}O_{10-z}$ with z varying between around 0.2 and 0.9 [28]. Formation of mullite was essentially due to dissolution of a small amount of Si into Al_2O_3 during the SHS process [29,30]. The yield of Fe_3Si as the only silicide phase under these two test conditions is justified by the fact that Fe_3Si exists in a composition range from 10 to 25 at.% Si. In view of no impurities in the final product, the Si-lean mixture of Fe-20 at.% Si was more favorable for the formation of Fe_3Si - Al_2O_3 composite.

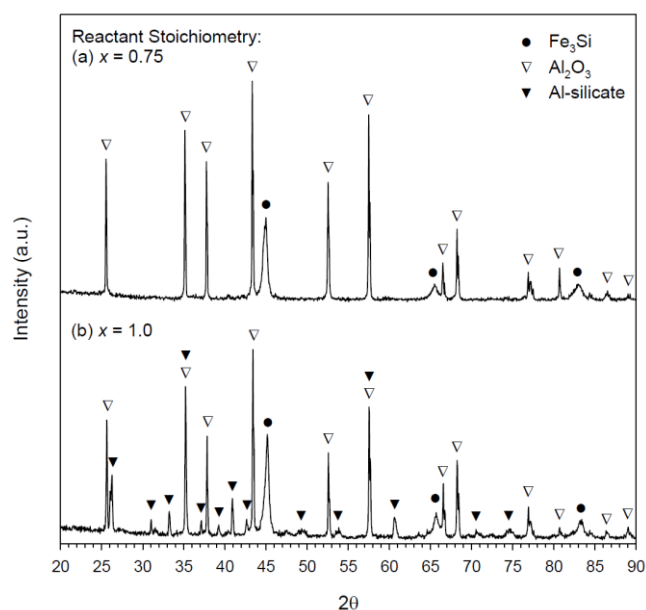


Figure 4. XRD patterns of Fe_3Si - Al_2O_3 composites synthesized from Reaction (1) with (a) $x = 0.75$ and (b) $x = 1.0$.

On account of its large negative Gibbs free energy change ($\Delta G^\circ = -840.8$ kJ) [24], the reaction pathways of Reaction (1) were proposed to be initiated by the aluminothermic reaction of $\text{Fe}_2\text{O}_3 + 2\text{Al} \rightarrow 2\text{Fe} + \text{Al}_2\text{O}_3$. In addition to the kinetic aspect, the reduction of Fe_2O_3 by Al was also a thermodynamically favored reaction which supplied a large amount of heat ($\Delta H_f^\circ = -852.3$ kJ) to maintain the synthesis reaction in the SHS mode. After the initiation step, the chemical interaction between Fe and Si proceeded to produce Fe_3Si .

For Reaction (1) with $x = 1.5$ and 2.0 (i.e., Fe-33.3% Si and Fe-40% Si), Figure 5a,b shows the presence of two silicide phases— Fe_3Si and FeSi —along with Al_2O_3 and aluminum silicate. The content of aluminum silicate appeared to be larger in the case of Fe-40% Si. Formation of Fe_3Si and FeSi was justified because of coexistence of both phases in the composition range from Fe-25 to Fe-50 at.% Si. Figure 5a,b indicates that the content of FeSi relative to Fe_3Si increases with increasing Si percentage. The strongest XRD peaks associated with FeSi and Fe_3Si are, respectively, located at $2\theta = 45.062^\circ$ (Inorganic Crystal Structure Database (ICSD) card number: 88-1298) and 45.337° (ICSD card number: 65-0994). It is believed that the addition of Si transformed a part of the Si-lean phase Fe_3Si to monosilicide FeSi , thus resulting in a decrease of Fe_3Si but an increase of FeSi . As proposed by Guan et al. [15], the reaction of Fe_3Si with additional Si generated an intermediate phase Fe_5Si_3 which further converted into the stable FeSi via the reaction of $\text{Fe}_5\text{Si}_3 + 2\text{Si} \rightarrow 5\text{FeSi}$.

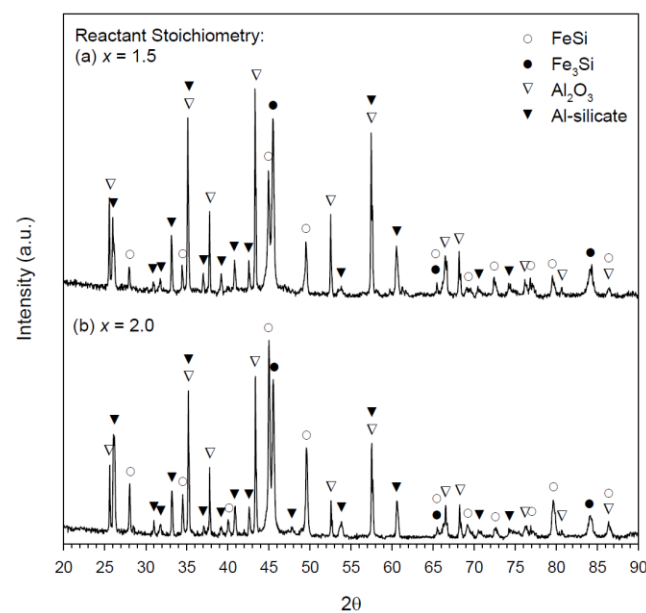


Figure 5. XRD patterns of $\text{Fe}_3\text{Si}/\text{FeSi}-\text{Al}_2\text{O}_3$ composites synthesized from Reaction (1) with (a) $x = 1.5$ and (b) $x = 2.0$.

Figure 6 presents the XRD spectrum of the product synthesized from Reaction (1) with $x = 3.0$ (i.e., Fe-50% Si). Apparently, monosilicide FeSi was the only silicide formed in the end product. Besides, Al_2O_3 and a small amount of aluminum silicate were detected. It should be noted that in spite of a high Si percentage, aluminum silicide is at a much less quantity in Figure 6 when compared with that in Figure 5. This could be explained by the fact that FeSi possesses a very narrow composition range. As a result, few Si particles dissolved in Al_2O_3 .

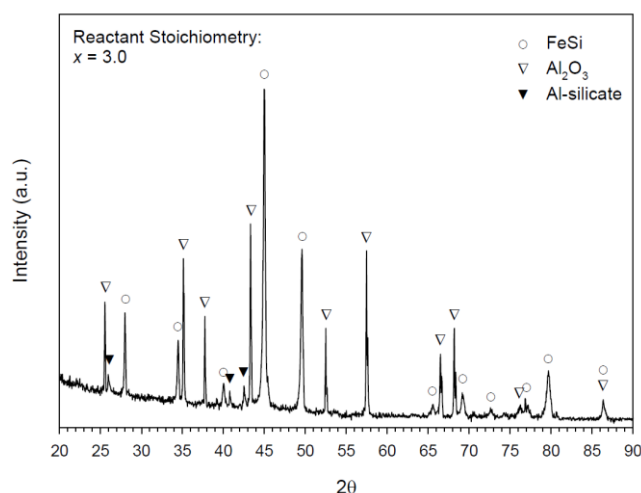


Figure 6. XRD pattern of FeSi-Al₂O₃ composite synthesized from Reaction (1) with $x = 3.0$.

Figure 7 presents an SEM image illustrating the fracture surface microstructure of the product synthesized from Reaction (1) with $x = 0.75$. The morphology features lots of granular particles distributing over the dense and connecting substrate. The EDS spectrum (a) indicates that the granular product is composed primarily of Fe and Si and has an atomic ratio of Fe/Si = 73.92/26.08 which is close to Fe:Si = 3:1. On the other hand, the EDS spectrum (b) shows that the dense substrate is made up of Al and O at a ratio of Al/O = 42.05/57.95. Therefore, it is believed that granular particles are Fe₃Si and the dense substrate is formed by Al₂O₃. Figure 7 also exhibits the particle size of Fe₃Si ranging approximately from 1 to 5 μm .

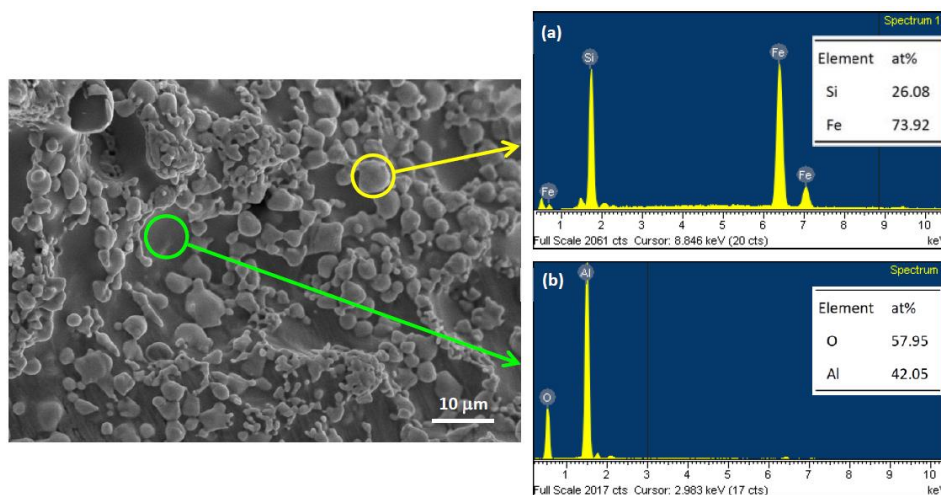


Figure 7. SEM image and EDS spectra associated with (a) Fe₃Si and (b) Al₂O₃ of SHS-derived product from Reaction (1) with $x = 0.75$.

The microstructure and elemental compositions of the product from Reaction (1) with $x = 1.5$ are shown in Figure 8. A similar morphology to that of Figure 7 was observed. The EDS analysis of two silicide grains selected in Figure 8 indicated that the intensity of Si peaks relative to that of Fe signals is stronger in the spectrum (a) than (b) and their respective atomic ratios are Fe/Si = 51.45/48.55 and 77.16/22.84. The former certainly is FeSi and the latter Fe₃Si. This verified the formation of both FeSi and Fe₃Si in the product of Reaction (1) with $x = 1.5$.

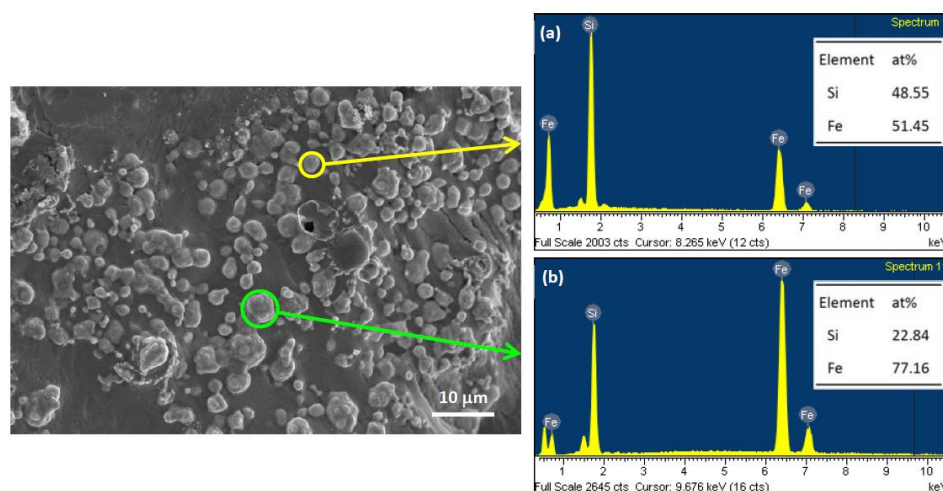


Figure 8. SEM image and EDS spectra associated with (a) FeSi and (b) Fe₃Si of SHS-derived product from Reaction (1) with $x = 1.5$.

The SEM image of Figure 9 was associated with the FeSi–Al₂O₃ composite synthesized from Reaction (1) with $x = 3.0$. Nearly spherical FeSi particles were identified with a size from submicron to around 2 μm. An atomic ratio of Fe/Si = 48.48/51.52 deduced from EDS spectrum (a) matched closely with the stoichiometry of FeSi. All four constituent elements were specified in EDS spectrum (b), among which the ratio of Al/O = 38.82/61.18 signifying Al₂O₃ was obtained.

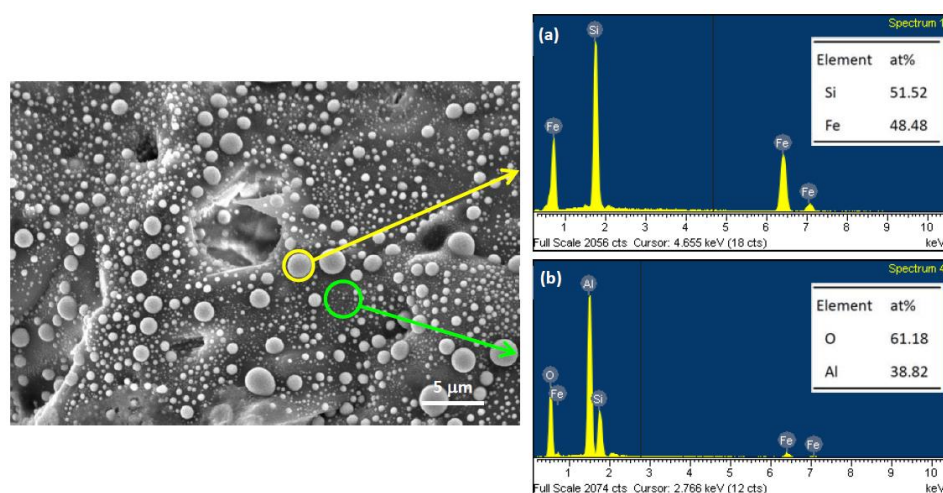


Figure 9. SEM image and EDS spectra associated with (a) FeSi and (b) Al₂O₃ of SHS-derived product from Reaction (1) with $x = 3.0$.

4. Conclusions

Fabrication of Fe₃Si/FeSi–Al₂O₃ composites was conducted by the aluminothermic SHS reactions with Fe₂O₃–Al–Fe–Si systems under Fe/Si stoichiometry from Fe-20 to Fe-50 at.% Si. Experimental results showed that self-propagating combustion was achieved upon ignition. The increase of Si percentage lowered combustion exothermicity and thus decreased not only the combustion front temperature from 1730 to 1506 °C, but flame-front velocity from 2.7 to 1.6 mm/s. Both Fe-20 and Fe-25 at.% Si reaction systems produced Fe₃Si–Al₂O₃ composites and the off-stoichiometric case with a Si-lean composition of Fe-20 at.% Si yielded almost no impurity, aluminum silicate. Two silicide phases—FeSi and Fe₃Si—were present in the final products of reaction systems with Fe-33.3 and Fe-40 at.% Si and the content of FeSi increased with increasing Si percentage. For the reaction with

Fe-50 at.% Si, the phase conversion was almost completed, and the product was FeSi–Al₂O₃ composite. SEM micrographs of the products revealed that Al₂O₃ formed a dense and connecting substrate, over which granular Fe₃Si and FeSi particles were uniformly distributed. The size of iron silicide particles varied in the range from submicron to 5 μm.

Author Contributions: Conceptualization, C.-L.Y.; methodology, C.-L.Y., K.-T.C. and T.-H.S.; validation, C.-L.Y., K.-T.C. and T.-H.S.; formal analysis, C.-L.Y., K.-T.C. and T.-H.S.; investigation, C.-L.Y. and K.-T.C.; resources, C.-L.Y.; data curation, C.-L.Y. and K.-T.C.; writing—original draft preparation, C.-L.Y., K.-T.C. and T.-H.S.; writing—review and editing, C.-L.Y.; supervision, C.-L.Y.; project administration, C.-L.Y.; funding acquisition, C.-L.Y. All authors have read and agreed to the published version of the manuscript.

Funding: This research work was funded by the Ministry of Science and Technology of Taiwan under the grant of MOST 110-2221-E-035-042-MY2.

Institutional Review Board Statement: Not applicable.

Informed Consent Statement: Not applicable.

Data Availability Statement: Data presented in this study are available in the article.

Conflicts of Interest: The authors declare no conflict of interest.

References

1. Murarka, S.P. Silicide thin films and their applications in microelectronics. *Intermetallics* **1995**, *3*, 173–186. [[CrossRef](#)]
2. Petrovic, J.J.; Vasudevan, A.K. Key developments in high temperature structural silicides. *Mater. Sci. Eng. A* **1999**, *261*, 1–5. [[CrossRef](#)]
3. Viennois, R.; Tao, X.; Jund, P.; Tedenac, J.C. Stability and thermoelectric properties of transition-metal silicides. *J. Electron. Mater.* **2011**, *40*, 597–600. [[CrossRef](#)]
4. Chirkin, A.D.; Lavrenko, V.O.; Talash, V.M. High-temperature and electrochemical oxidation of transition metal silicides. *Powder Metall. Metal. Ceram.* **2009**, *48*, 330–345. [[CrossRef](#)]
5. Chen, X.; Liang, C. Transition metal silicides: Fundamentals, preparation and catalytic applications. *Catal. Sci. Technol.* **2019**, *9*, 4785–4820. [[CrossRef](#)]
6. Kauss, O.; Obert, S.; Bogomol, I.; Wablat, T.; Siemensmeyer, N.; Naumenko, K.; Krüger, M. Temperature Resistance of Mo₃Si: Phase stability, microhardness, and creep properties. *Metals* **2021**, *11*, 564. [[CrossRef](#)]
7. Dahal, N.; Chikan, V. Phase-Controlled synthesis of iron silicide (Fe₃Si and FeSi₂) nanoparticles in solution. *Chem. Mater.* **2010**, *22*, 2892–2897. [[CrossRef](#)]
8. Wu, J.; Chong, X.Y.; Jiang, Y.H.; Feng, J. Stability, electronic structure, mechanical and thermodynamic properties of Fe-Si binary compounds. *J. Alloys Compd.* **2017**, *693*, 859–870. [[CrossRef](#)]
9. Kubaschewski von Goldbeck, O. *Iron-Binary Phase Diagrams*; Springer-Verlag: Berlin/Heidelberg, Germany, 1982; pp. 136–139.
10. Zhang, Y.; Ivey, D.G. Fe₃Si formation in Fe-Si diffusion couples. *J. Mater. Sci.* **1998**, *33*, 3131–3135. [[CrossRef](#)]
11. Gras, C.; Gaffet, E.; Bernard, F.; Niepce, C.J. Enhancement of self-sustaining reaction by mechanical activation: Case of an Fe-Si system. *Mater. Sci. Eng. A* **1999**, *264*, 94–107. [[CrossRef](#)]
12. Gras, C.; Bernsten, N.; Bernard, F.; Gaffet, E. The mechanically activated combustion reaction in the Fe-Si system: In situ time-resolved synchrotron investigations. *Intermetallics* **2002**, *10*, 271–282. [[CrossRef](#)]
13. Gras, C.; Zink, N.; Bernard, F.; Gaffet, E. Assisted self-sustaining combustion reaction in the Fe-Si system: Mechanical and chemical activation. *Mater. Sci. Eng. A* **2007**, *456*, 270–277. [[CrossRef](#)]
14. Zakeri, M.; Rahimpour, M.R.; Sadmezhad, S.K. In situ synthesis of FeSi–Al₂O₃ nanocomposite powder by mechanical alloying. *J. Alloys Compd.* **2010**, *492*, 226–230. [[CrossRef](#)]
15. Guan, J.; Chen, X.; Zhang, L.; Wang, J.; Liang, C. Rapid preparation and magnetic properties of Fe₃Si–Al₂O₃ nanocomposite by mechanical alloying and heat treatment. *Phys. Status Solidi A* **2016**, *213*, 1585–1591. [[CrossRef](#)]
16. Li, M.; Chen, X.; Guan, J.; Wang, J.; Liang, C. Thermally induced phase transition and magnetic properties of Fe–FeSi₂ with core–shell structure. *Phys. Status Solidi A* **2013**, *210*, 2710–2715. [[CrossRef](#)]
17. Yeh, C.L.; Chen, K.T. Synthesis of FeSi–Al₂O₃ composites by autowave combustion with metallothermic reduction. *Metals* **2021**, *11*, 258. [[CrossRef](#)]
18. Yeh, C.L.; Chen, K.T. Fabrication of FeSi/α-FeSi₂-based composites by metallothermically assisted combustion synthesis. *J. Aust. Ceram. Soc.* **2021**. [[CrossRef](#)]
19. Merzhanov, A.G. Combustion processes that synthesize materials. *J. Mater. Process. Technol.* **1996**, *56*, 222–241. [[CrossRef](#)]
20. Bertolino, N.; Anselmi-Tamburini, U.; Maglia, F.; Spinolo, G.; Munir, Z.A. Combustion synthesis of Zr-Si intermetallic compounds. *J. Alloys Compd.* **1999**, *288*, 238–248. [[CrossRef](#)]

21. Yeh, C.L.; Chen, W.H. Combustion synthesis of MoSi₂ and MoSi₂-Mo₅Si₃ composites. *J. Alloys Compd.* **2007**, *438*, 165–170. [[CrossRef](#)]
22. Yeh, C.L.; Peng, J.A. Combustion synthesis of MoSi₂-Al₂O₃ composites from thermite-based reagents. *Metals* **2016**, *6*, 235. [[CrossRef](#)]
23. Maung, S.T.M.; Chanadee, T.; Niyomwas, S. Two reactant systems for self-propagating high-temperature synthesis. *J. Aust. Ceram. Soc.* **2019**, *55*, 873–882. [[CrossRef](#)]
24. Binnewies, M.; Milke, E. *Thermochemical Data of Elements and Compounds*; Wiley-VCH Verlag GmbH: Weinheim, Germany, 2002.
25. Acker, J.; Bohmhammel, K.; van den Berg, G.J.K.; van Miltenburg, J.C.; Kloc, C. Thermodynamic properties of iron silicides FeSi and α-FeSi₂. *J. Chem. Thermodyn.* **1999**, *31*, 1523–1536. [[CrossRef](#)]
26. Yeh, C.L.; Lin, J.Z. Combustion synthesis of Cr-Al and Cr-Si intermetallics with Al₂O₃ additions from Cr₂O₃-Al and Cr₂O₃-Al-Si reaction systems. *Intermetallics* **2013**, *33*, 126–133. [[CrossRef](#)]
27. Wang, L.L.; Munir, Z.A.; Maximov, Y.M. Thermite reactions: Their utilization in the synthesis and processing of materials. *J. Mater. Sci.* **1993**, *28*, 3693–3708. [[CrossRef](#)]
28. Schneider, H.; Schreuer, J.; Hildmann, B. Structure and properties of mullite—A review. *J. Eur. Ceram. Soc.* **2008**, *28*, 329–344. [[CrossRef](#)]
29. Zaki, Z.I.; Mostafa, N.Y.; Ahmed, Y.M.Z. Synthesis of dense mullite/MoSi₂ composite for high temperature applications. *Int. J. Refract. Met. Hard Mater.* **2014**, *45*, 23–30. [[CrossRef](#)]
30. Yeh, C.L.; Chou, C.C. Formation of NbB₂/mullite composites by combustion synthesis involving metallothermic reduction of Nb₂O₅ and B₂O₃. *Ceram. Int.* **2015**, *41*, 14592–14596. [[CrossRef](#)]